ORIGINAL RESEARCH ARTICLE

Microstructural Changes During Short-Term Heat Treatment of Martensitic Stainless Steel—Simulation and Experimental Verification

N. SCHMIDTSEIFER and S. WEBER

Short-term heat treatments of steels are used for tools and cutlery but also for the surface treatment of a variety of other workpieces. If corrosion resistance is required, martensitic stainless steels like AISI 420L or AISI 420MoV are typically used. The influence of short-term heat treatment on the different metastable states of the AISI 420L steel was examined and reported in this article. Starting from a defined microstructural state, the influence of a short-term heat treatment is investigated experimentally with the help of a quenching dilatometer and computer assisted simulations are carried out. With the results obtained, a simulation model is built up which allows to compute the microstructural changes during a short-term heat treatment to be evaluated without the need for an experiment. As an indicator, the value of the martensite start temperature is calculated as a function of different holding times at austenitizing temperature. The martensite start temperature is measured by dilatometry and compared to calculated values. Validation of simulated results reveals the potential of optimizing steel heat treatment processes and provides a reliable approach to save time, resources and energy.

https://doi.org/10.1007/s11661-021-06280-y

I. INTRODUCTION

TOOL steels are used when special challenges are posed to the properties of the material. In many cases, high hardness and good corrosion resistance are of great importance, so corrosion-resistant martensitic steels are used. Applications are, for example, knives, medical products, scissors or even razor blades. The most important alloying element, besides carbon, is chromium. Chromium can passivate the metallic matrix and thus protect it from corrosive attacks. However, chromium must be dissolved in the matrix and should not be bound in carbides to provide matrix corrosion resistance. The lower limit value is a content of 12 wt pct chromium.[1] By heat treatment, chromium can be dissolved in the matrix and thus provide corrosion resistance.[2] For this purpose existing carbides must be dissolved. In this way, also carbon is released to the fcc matrix, providing hardenability. The carbides in turn contribute to the strength and hardness of the steel. It is therefore necessary to find a good compromise in order to obtain a hard, corrosion-resistant steel that meets all requirements. Conventional heat treatments of martensitic stainless steels are carried out in four steps in the simplest case.[2] First, the workpiece is heated to an austenitizing temperature, then kept at this temperature for a defined time and finally quenched in a defined manner. The fourth and last step is tempering. Overall, the processes are very lengthy and often take several hours. Depending on the intended use, the heat treatments vary to a great extent. In the case of pliers, for example, only the flanks that are in engagement are hardened by a surface heat treatment. The required properties, such as high hardness and good corrosion resistance, are achieved on the functional surfaces. In the case of razor blades, they are completely heat treated, but the volumes that are heated are very small, since razor blades are only a few 100 μm thick. In both cases only little volumes of material are heated, and so-called short-term heat treatments are used, in which the material is only kept at austenitizing temperature for seconds or a few minutes. These short times are sufficient for martensitic hardening, since no thermodynamic equilibrium of the multiphase system is aimed at, but quenching is carried out from a metastable equilibrium. In this context, it has to be considered that dissolution kinetics of Cr carbides are by far slower

N. SCHMIDTSEIFER is with the Fakultät für Maschinenbau und Sicherheitstechnik, Lehrstuhl für Neue Fertigungstechnologien und Werkstoffe, Bergische Universität Wuppertal, 42651 Solingen, Germany. Contact e-mail: schmidtseifer.fuw@uni-wuppertal.de S. WEBER is with the Institut für Werkstoffe, Lehrstuhl Werkstofftechnik, Ruhr-Universität Bochum 44780, Bochum, Germany.

Manuscript submitted October 21, 2020; accepted April 1, 2021.
Article published online April 28, 2021

compared to the dissolution of cementite in a plain carbon steel.[3,4]

There are several studies about the processes during heat treatment, especially the processes during dissolution or formation of carbides. Garcia *et al.* investigated the effects of the heat treatment parameters on the processes of transformation in nonequilibrium conditions for the steel AISI 420C (X45Cr13) and similar grades.[5] Among other aspects, the heating and cooling rates and the austenitizing temperature were varied and the changes in carbide distribution, resulting hardness and grain size were investigated. The heating and cooling rates used varied between 0.5 and 25 K s^{-1}. However, significantly higher rates are used for short-term heat treatment. The influence of the cooling rate on the local chromium depletion in the steels X20Cr13 and X46Cr13 was investigated by Rosemann *et al.*[6] Face quenching tests were employed for their investigations. Here, a cooling rate of up to 400 K s^{-1} is achieved at the front face. The authors focused their work on corrosion resistance and did not vary the austenitizing conditions. *Schneider and Inden* simulated the processes of phase transformations in ferritic/martensitic steels.[7] They also considered short times such as 10 seconds austenitizing time. The results were only simulated but not compared with experiments. These and other studies suggest that the processes in a short-term heat treatment can be similar to those for conventional heat treatments. However, there are no studies that have been able to show this similarity.

In the following, the transferability of the individual approaches for the processes taking place during a heat treatment to a short-term heat treatment is examined and presented. In any case, it is important to have a precise knowledge of the initial state—usually a soft annealed condition—for the short-term heat treatment. This knowledge is all the more important for the investigations shown here in order to be able to judge whether the simulation models set up are able to reproduce the real processes.

II. EXPERIMENTAL PROCEDURE

The material under investigation is an AISI 420L (X20Cr13). The chemical composition was determined with an optical emission spectrometer and is shown in Table I. Samples are used which have the necessary dimensions for experiments in a quench dilatometer. These are hollow cylindrical specimens with an outer diameter of 4 mm and a length of 10 mm. For a reduction of the volume and to be able to implement high heating and quenching rates, a 2 mm bore was drilled axially.

First investigations have shown a large difference in the microstructure of the available batches in the as-delivered state. Figure 1 shows two different batches of the steel AISI 420L (X20Cr13). Both states are metallographically prepared and etched with V2A pickling at room temperature (V2A pickling: 100 ml HCl, 100 ml H_2O, 10 ml HNO_3). Figure 1 left shows a ferritic matrix with uniformly distributed fine precipitates. The etching time for this sample was about 10 seconds. The sample in Figure 1 right was prepared in the same way. The microstructure also shows a ferritic matrix, but the precipitates have been removed from the matrix by etching. In order for this to happen, the etching must have been accompanied by a major attack by the acid in the areas around the precipitates. The reason for this is a local depletion of chromium in the matrix, as the corrosion resistance has been reduced locally.[6] This result implies the necessity of producing a representative initial state first.

To achieve a representative initial state, the steel samples were subjected to an austenitizing temperature of 1100 °C for 1 hour with subsequent quenching in still oil to achieve a precipitate-free microstructural state. This was followed by long-term tempering to precipitate defined carbides for 240 hours at 750 °C without defined atmosphere in a muffle furnace. Again, quenching in oil was performed. All heat treatments following the defined initial state were carried out in a quenching dilatometer. All samples were heated to an austenitizing temperature T_{stht} of 1000 °C. The heating rate was 250 K s^{-1} in each test, while the quenching rate was kept constant at − 121.25 K s^{-1}. A helium partial pressure of 0.8 bar was set for each test to create an inert environment to prevent oxidation, while quenching was performed with nitrogen. Thus, all parameters were constant except for the austenitizing time t_{stht}. The austenitizing time was varied in the following steps: 0 seconds, 5 seconds, 10 seconds, 30 seconds, 60 seconds, 5 minutes, 10 minutes, 60 minutes. Figure 2 shows a schematic temperature curve of the different heat treatment steps.

To evaluate the dilatometer data, the second derivative of the change in length over temperature was examined. This allows transformation points to be determined precisely by identifying large deviations from the zero line. This method was used to determine the martensite start temperature as a function of the austenitization time in order to compare it with the results of the simulation. All samples were metallographically prepared to reveal the microstructure. For this purpose, the specimens were embedded in a electrically conducting resin and polished in several steps down to 1 μm and then etched with V2A pickling at room temperature. The samples were examined with a scanning electron microscope at different magnifications in secondary electron imaging mode. All simulations were performed with the commercial software MatCalc 6.02 (rel 1.003). In any case, the simulation started with the one-phase complete solution state of the austenite at 1100 °C. Thus all simulations start with the setting of the precipitation-free state analogous to the experimental tests in the dilatometer. The long-term tempering for the precipitation of the carbides was represented in the simulation model with the same parameters. The short-term heat treatments, which were also carried out with the quenching dilatometer, were also considered in the simulation with the parameters similar to the experimental parameters.

Table I. Chemical Composition of the Examined Material AISI 420L (X20Cr13)

	C*	Cr*	Ni*	Mn*	Si*	Mo	V	S	P	Fe*
MW	0.207	12.62	0.244	0.501	0.433	0.069	0.021	0.025	0.025	bal.
SD	0.015	0.098	0.005	0.009	0.017	0.001	0.001	0.001	0.001	

All measurements were performed with an optical emission spark spectrometer. All values in mass pct. The star (∗) specifies which elements were taken into account in the simulation. (MW - mean weight; SD - standard deviation).

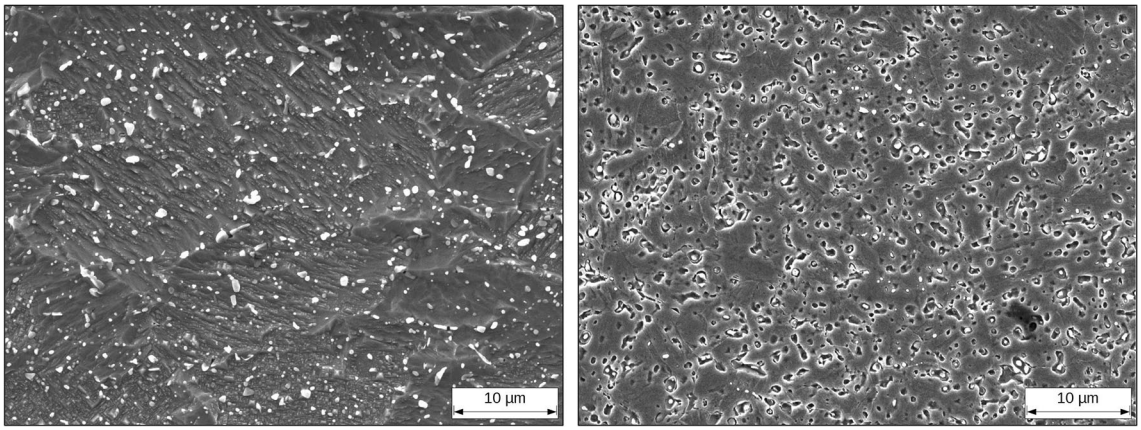

Fig. 1—Two different batches of the steel AISI 420L (X20Cr13). Left: Charge A, polished and etched for 10 s. Right: Charge B, polished and etched for 1 s.

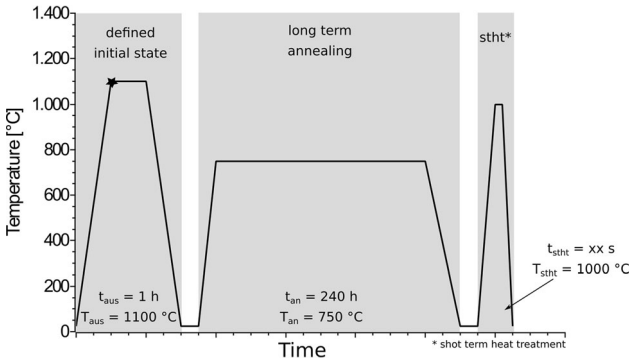

Fig. 2—Schematic temperature curve of the heat treatment. The star marks the starting point for the simulation.

III. RESULTS AND DISCUSSION

First, the defined initial state was set. Figures 3 and 4 show the two steps required for this. Figure 3 shows the precipitate-free martensitic state after solution annealing for one hour at 1100 °C followed by oil-quenching in a magnification of ×5000. In this state the samples have a hardness of 565 ± 5.1 HV10. Deep cryogenic treatment (DCT) in liquid nitrogen for 30 minutes and measuring the hardness again shows no further increase in hardness in previous experiments. This may suggest that no retained austenite has remained and the material is in a fully martensitic state in which all alloying elements are dissolved in the matrix even after conventional oil-quenching. Figure 4 shows the microstructural state after long-term tempering for 240 hours at ×5000 magnification. A tempered ferritic matrix and precipitated carbides can be seen. These have precipitated on the habit planes of the original martensite needles and along the grain boundaries. Precipitates inside former martensite needles are not visible. XRD investigations show that all the carbides present are of the $M_{23}C_6$ type. With reference to the determined 2-Θ-angles, the chemical composition of these $M_{23}C_6$ carbides can be determined as: 5.6 wt pct carbon, 64.3 wt pct chromium and 30.2 wt pct iron.

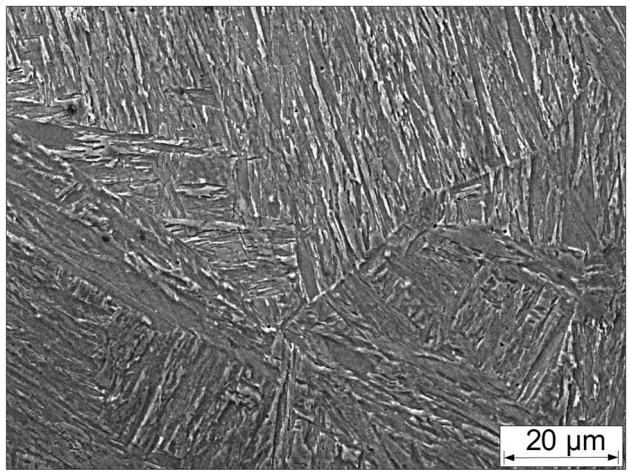

Fig. 3—Fully martensitic matrix without precipitates after solution heat treatment at 1100 °C plus quenching in oil.

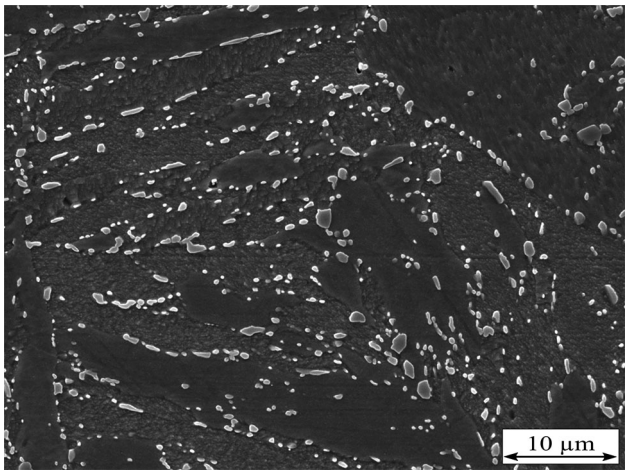

Fig. 4—Structure of the defined initial state. Ferritic matrix with precipitated $M_{23}C_6$ carbides after tempering at 750 °C for 240 h and oil-quenching.

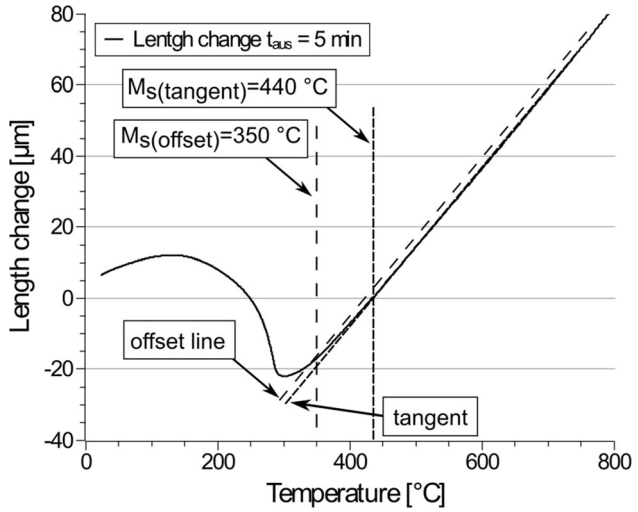

Fig. 5—Course of the change in length in the cooling curve after austenitizing for 5 minutes at 1000 °C. The evaluation methods of the offset method[14] and the tangent method according to Ref. 13 are also shown.

A. *Determination of Martensite Start*

In all of the tests described here, the determination of the M_s temperature on the basis of the measured values of the dilatometric experiments was noticeable. In the literature different possibilities of evaluation are described and evaluated.[8–12] When looking at the change in length during cooling after austenitizing for 5 minutes with different evaluation methods something is noticeable which cannot be explained directly. With a few of the usual evaluation methods, incorrect martensite start temperatures would be determined. In order to evaluate this in more detail, various evaluation methods are presented below. The simplest and fastest way is the method according to ASTM A1033-18.[13] In this case, a tangent is applied directly to the signal of the change in length in the regime of the austenite. From high temperatures to lower temperatures, the tangent and the trace are compared. The point at which the curve of the measured values first breaks the tangent in the direction of positive length change is read off as the M_s temperature on the abscissa. A graphical representation of this method is shown in Figure 5. Here it can also be seen that an M_s temperature of 440 °C is determined with this method.

Another method, which is shown in Figure 5 and also works directly with the measurement signal of the length change, is the offset method according to Yang and Bhadeshia.[14] With this method, a tangent is also first applied to the measurement signal in the area of the austenite. In the next step, however, this tangent is provided with an offset which shifts the tangent vertically in the direction of positive length changes. The amount of the offset is calculated using the lattice parameters of austenite and martensite, taking into account the dissolved alloying elements. The point at which the measurement signal and the offset line intersect is then read off to the abscissa as the M_s temperature. Figure 5 shows an example of this procedure. The offset line was drawn arbitrarily for the representation. The real calculated offset amount is smaller, such that the shift would not be visible. With this simplified shift, an M_s temperature of 350 °C would be determined. An exact application of the offset method yields an M_s temperature of 387 °C for this experiment.

Two further methods investigate derivatives of the change in length over temperature. The procedure for determining M_s is identical in both cases. The first or second derivative is plotted over temperature. The course of these graphs is approximated by a horizontal straight line in the regime of high temperatures, in the stability range of austenite. In these cases, the graphs are also read from high temperatures in the direction of lower temperatures. The point at which the first derivative of the change in length leaves the horizontal in a negative direction is also read off here on the abscissa as M_s. Kamyabi-Gol *et al.*[10] also used this method to evaluate further phase transformations and structural changes. In Figure 6 this procedure is shown again for the previously investigated experiment. Using the method after the first derivation yields an M_s temperature of 448 °C. In comparison to the tangent method according to Reference 13 shown above, the results are comparable. In contrast, the offset method according to Reference 14 yields a significantly lower M_s temperature. If the temperatures determined with the three different methods for martensite start are compared with the values from literature, it becomes clear that all values were too high. For example in literature there are values for M_s given for AISI 420L with 300 °C[15] or 253 °C[16] With the knowledge of these large differences, the second derivative of the change in length was investigated as a further variant. The general procedure was approximated to that used to investigate the first derivative. The only difference here is that the point is searched on the graph of the second derivative leaving the horizontal line for the first time in positive direction. The procedure is also shown in Figure 6. This evaluation method results in a significantly lower martensite start

temperature of 296 °C. The results already presented before clearly show that this variant of evaluation in the tests presented here provides temperatures for martensite start which are comparable with both literature and simulation results. The question remains, why in these investigations the well-known and frequently used methods described above provide supposedly results with a wide difference. In order to be able to compare the methods directly, the results of all investigations are summarized in Table II.

The work mentioned above has applied and evaluated the different methods in their articles.[8] In many papers two phenomena are described in this context, which could also explain the anomalies in this work. First the so-called *splitting phenomenon* is reported.[11,17,18] Figure 7 shows a schematic representation of the *splitting phenomenon* as it is illustrated in a dilatometer curves of the change in length.[17] Here it can be seen that the curve of length change does not allow exactly one point to be determined as M_s temperature using, for example, the tangent method. A point M_{sII} is shown, which already gives a deviation of the measured values from the tangent at higher temperatures. The occurrence of M_{sII} is explained by References 17, 18 with the elimination of carbides. The cooling rate applied in the experiments investigated by Garcia *et al.* was − 50 K s^{-1}.[18] In the experiments conducted in this work the cooling rate was − 121.25 K s^{-1}. This means that during the cooling process there is considerably less time available for possible precipitation. The alloys investigated in Reference 18 also contained significantly larger quantities of alloying elements, which significantly increased the driving force for precipitation.[19] Marcuci *et al.*[11] also investigated materials similar to AISI 420L (X20Cr13) with the steels ASTM 420A (X45Cr13) and ASTM440C. In their work cooling rates of up to 500 K s^{-1} were implemented.[11] In their experiments they also detected the *splitting phenomenon*, but only with austenitizing temperatures that are not in the range of homogeneous austenite. Therefore, they concluded that the *splitting phenomenon* is mainly dependent on the distribution of carbon in the matrix of the austenite. At higher austenitizing temperatures, the austenite is more homogeneous. The more homogeneous the austenite, the smaller the *splitting phenomenon*. At very high temperatures the phenomenon does not occur at all. In summary, according to Marcuci *et al.*, the *splitting phenomenon* occurs with unequally distributed carbon in the matrix or with the presence of carbides.[11] However, no experiment in this current study showed such a *splitting phenomenon*. Therefore, it is assumed that existing carbon gradients must be larger than the present ones to cause a splitting phenomenon.

The second frequently mentioned phenomenon is the *slow start* phenomenon.[9,10] In general, this phenomenon also refers to an early deviation from an established tangent. A *slow start* is characterized by a

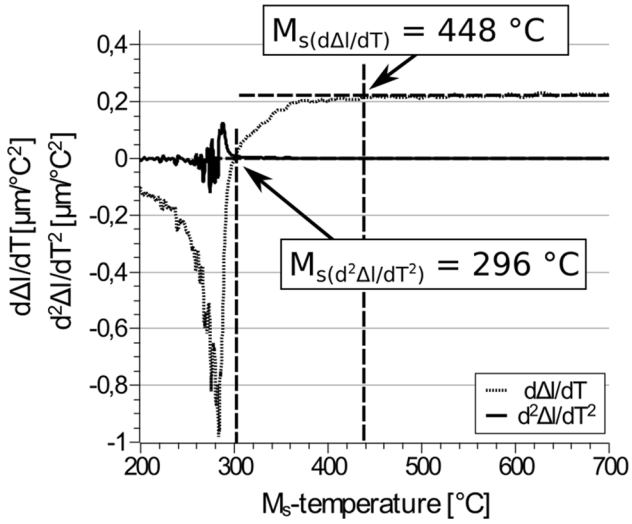

Fig. 6—Course of the first and second derivation of the length change over temperature (t_{aus} = 5 min, T_{aus} = 1000 °C). The straight lines show the reading of the martensite start temperature at the respective courses.

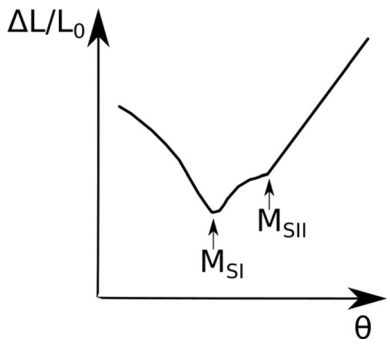

Fig. 7—Dilatometric representation of the splitting phenomena in the martensitic transformation adapted from Ref. [17].

Table II. Determined Martensite Start Temperatures According to the Different Methods Presented

T_{aus}	0 s	5 s	10 s	30 s	1 min	5 min	10 min	Source
Tangent	394 (17)	332 (43)	336 (14)	323 (23)	396 (19)	400 (13)	393 (15)	13
Offset	390 (19)	345 (14)	363 (9)	368 (18)	395 (9)	368 (17)	352 (42)	14
1. Derivation	413 (33)	374 (*)	353 (14)	332 (16)	342 (17)	390 (50)	391 (78)	10
2. Derivation	401 (14)	343 (14)	329 (9)	324 (3)	326 (12)	323 (35)	285 (23)	—

All values in °C, the values in brackets indicate the respective standard deviation. The star (*) indicates that not enough measured values were recorded.

continuous change of the slope. In comparison, Figure 7 shows that after the critical point in a *splitting phenomenon*, the curve after the critical point continues with the same gradient as before until M_sI is reached. A *slow start*, on the other hand, is indicated by the progression of the measured values as shown in Figure 5. *Sourmail and Smanio* discuss three different possible explanations for a *slow start*.[9] The first possibility for the occurrence of the phenomenon is a difference in the local chemical composition. According to their investigations, this can only explain small deviations of 4 K maximum. According to Reference 9, another possible cause for a *slow start* could be a different grain size of the original austenite. But even this approach can only be the reason for a deviation of 4 K to 5 K. As a last possibility a temperature gradient occurring within the sample was labeled. *Sourmail and Smanio* have performed experiments with several thermocouples on one sample and were able to measure a deviation in the resulting M_s-temperatures within a sample of 5 K to 10 K. In each case the ends of the sample are converted first. However, all three factors can only explain deviations between two supposedly occurring M_s-temperatures of up to 10 K. In this work deviations up to 77 K were measured (t_{aus} = 5 min, Table II). Another conspicuousness documented in Reference 9 is that the phenomenon is not reproducible. Sourmail and Smanio suggest that heat exchange conditions are most likely to cause a *slow start*. So neither the sample nor the geometry of the sample would be involved in the *slow start* phenomenon, but the cooling conditions are primarily responsible for it. Under these circumstances, the offset method according to Yang and Bhadeshia[14] should not be used, because this method reacts very sensitively to first changes in the cooling curve and thus leads to incorrect evaluations.[9] Also Kamyabi-Gol *et al.*[8] proved in another work that the offset method[14] often produces results that are too high. As a justification, they refer to the determination of the offset, where single alloying elements with their specific lattice distortions are taken into account, but not all possible alloying elements such as copper are included. It was noted that the manually created tangent is another source of error.[8] In a previous work, Kamyabi-Gol *et al.*[10] investigated the accuracy of the method after the first derivative compared to mathematical models for independent quantification of phase quantities in different phase transformations. It was shown that this method yielded well-matched values for M_s. However, these results are only valid if the measured values do not show a *slow start*.[10] *Olson and Owen* present a detailed discussion of the nucleation of martensite.[20] They describe various influences on martensite nucleation and divide it into three main groups. First: Relaxation of the (sub-)structure or the microstructure. Second: Heterogeneity with respect to defects. And thirdly: direction of stress of the deformation. These influences determine the predominant energies necessary to enable martensite nucleation. They divide the nucleation into three models based on these energies: classical, nonclassical and quasiclassical. These models are not static and often merge into one another.[20] If one refers the previously presented work to the results shown in this paper, it becomes clear that the experiments, exemplarily considered on cooling after t_{aus} = 5minutes, show a course which cannot be called a *splitting phenomenon*. The course of the length change in Figure 5 shows a continuous change of the slope until the M_s temperature is reached. In addition, large cooling rates have been used to severely limit or prevent carbide precipitation during cooling. Therefore, the processes recorded with the dilatometer are considered to show a *slow start* phenomenon. An exact explanation of the causes of this phenomenon is very difficult and has not been clearly clarified in the literature so far. Overall, the cooling conditions and also the nucleation mechanisms regarding to the chemical composition of martensite need to be investigated in more detail for an explanation.[10,20,21] A comparison of the different evaluation methods Tangent,[13] Offset,[14] first derivative[10] and second derivative with consideration of the deviation of the individual results shows that the method of the second derivative in this work provides reliable results also in connection with the simulation results. Especially when a *slow start* is visible in the measured values, this evaluation method yields reliable M_s-temperatures, which also corresponds to literature 15, 16.

B. *Dilatometry and Martensite Start*

The martensite start temperature was experimentally determined by quenching dilatometry. For this purpose, the second derivative of the measurement signal of the length change over temperature was determined and analyzed, according to the preliminary investigations described before. At the point where the measurement signal first shows a positive deviation from the horizontal line of the derivative, the martensite start temperature is read. Figure 8 shows this procedure as an example for the test with an austenitizing time of 5 minutes at 1000 °C. The martensite start temperatures determined in this way with the associated standard deviations are shown in Table III. First of all, a sharp

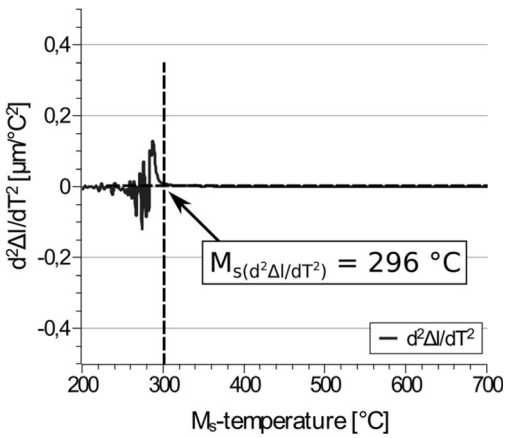

Fig. 8—Second derivation of the change in length of the cooling curve after austenitizing for 5 minutes at 1000 °C. The dashed lines are indicating the graphical determination of the M_s-temperature.

Table III. Experimentally M_s-Temperatures (in °C) and Corresponding Standard Deviation Determined as the Second Derivation of the Change in Length Over Temperature

t_{aus}	0 s	5 s	10 s	30 s	60 s	5 min	10 min	60 min
M_s-MW	377	333	326	319	314	286	278	281
M_s-SD	10	2	4	6	10	10	12	10

drop in the M_s-temperatures from 377 ± 10 °C ($t_{aus} = 0s$) to 286 ± 10 °C ($t_{aus} = 5$minutes) can be seen. If the austenitizing time is extended to 60 minutes, the measured temperature drops only slightly to 281 ± 10 °C.

C. *Hardness*

Hardness measurements according to Vickers HV10 show that with increasing austenitizing time the hardness also increases steadily. After long-term tempering (240 hours, 750 °C), the specimens exhibit a hardness of 419 ± 13.5 HV10. If the sample is not kept at the austenitizing temperature during the short-term heat treatment, but quenched again immediately after reaching this temperature, a hardness of 410 ±4.8 HV10 is achieved. This clearly shows that the heating rate was selected sufficiently high so that no changes in the carbides occur during heating. Since no additional carbon is provided, there can be no increase in hardness.[1,19] The hardness initially increases rapidly with increasing austenitizing time. After one minute at austenitizing temperature the hardness is 509 ± 5.9 HV10. If the sample remains at 1000 °C for one hour, the hardness increases further to 712 ± 9.1 HV10. Figure 9 shows a graphical representation of the hardness values determined as a function of the austenitizing time. In the course of the hardness, the co-relation between carbide dissolution and hardness increase resulting from increasing matrix carbon levels is well visible. This shows the direct relationship between the carbon content and the resulting hardness in martensitic hardening.

D. *Microstructure*

The samples with the carbides in initial state conditions, which can be seen in Figure 4, were heat treated in the quenching dilatometer at different austenitizing times. Figure 10 shows four different conditions, each with different austenitizing times of 1, 5, 10, and 60 minutes. All samples show carbides except for the 60 min conditions. With increasing austenitizing time the number of carbides decreases and in parallel, C- and Cr levels within the matrix increase. None of the samples has a preferred direction of microstructure, therefore the surface area of the carbides in the images can be directly gauged to the phase fraction. Digital image analyses show that the phase fraction of the carbides is 3.64 ± 0.01 vol pct for an austenitizing time of 1 minute. After an austenitizing time of 5 minutes the phase

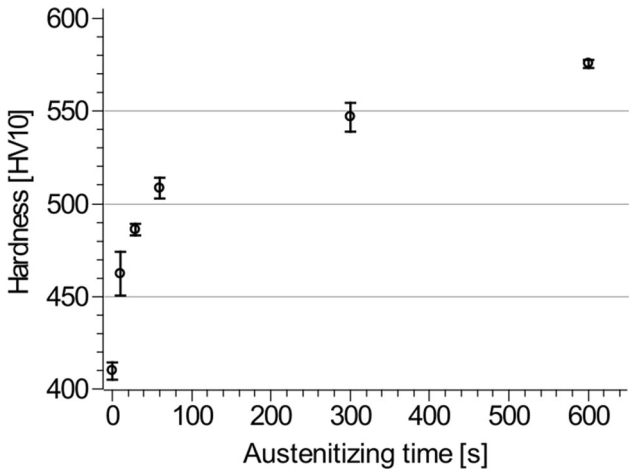

Fig. 9—Measured hardness values in HV10 as a function of the austenitizing time for austenitizing at 1000 °C.

fraction is still 1.81 ±0.68 vol pct and after 10 minutes the carbides take up a fraction of 1.08 ± 0.22 vol pct.

E. *Simulation of Phase Fraction and Chemical Composition*

All heat treatments performed experimentally were also simulated with the same parameters with MatCalc. After tempering for 240 hours, the simulated phase fraction of $M_{23}C_6$ is 0.04523. This value agrees well with the thermodynamic equilibrium quantity for 750 °C. When heating during the short-term heat treatment, the heating rate was selected so high that a transformation or dissolution of the precipitates could be prevented to a large extent (250 K s^{-1}). According to the calculations, the proportion of precipitates during heating is reduced to 0.04504. When maintained at 1000 °C, the precipitates dissolve under diffusion control and the phase fraction thus decreases. The simulation results of this dependence are shown in Figure 11. The phase fraction of $M_{23}C_6$ decreases continuously until after about 27 minutes all precipitates are dissolved and the phase fraction thus reaches 0. After this, only austenite remains in the microstructure, isothermally at 1000 °C.

The chemical composition of the austenite at hardening temperature depends directly on the remaining phase quantities of carbides under the assumption that C and Cr are distributed homogenously within the fcc phase during austenitizing.[22] As the carbides dissolve, the

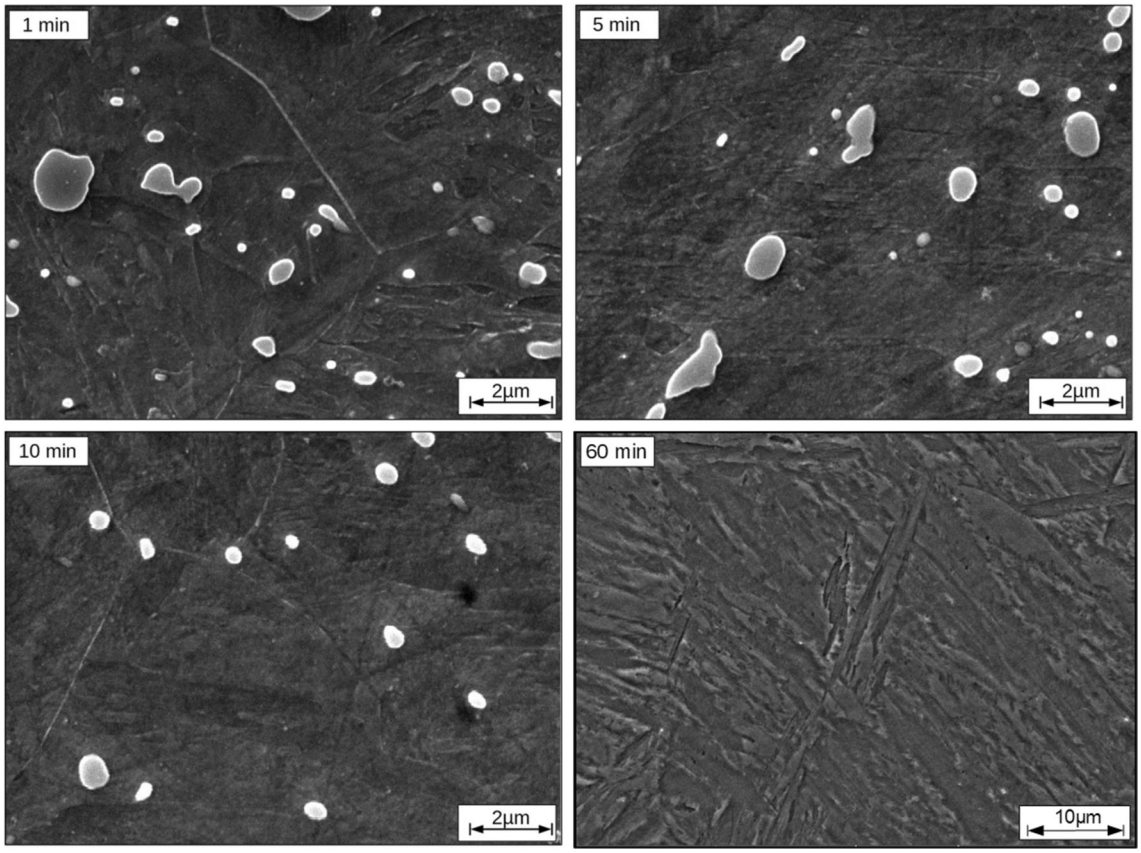

Fig. 10—Different microstructures after short-term heat treatment in the dilatometer. Top left: $t_{aus} = 1$ min, top right: $t_{aus} = 5$ min, bottom left: $t_{aus} = 10$ min, bottom right $t_{aus} = 60$ min. All samples are etched.

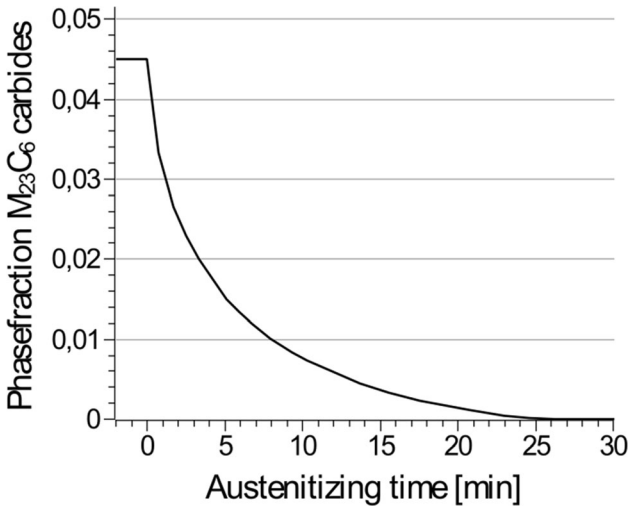

Fig. 11—Simulated phase fraction of $M_{23}C_6$ carbides in austenite as a function of austenitizing time in minutes at 1000 °C.

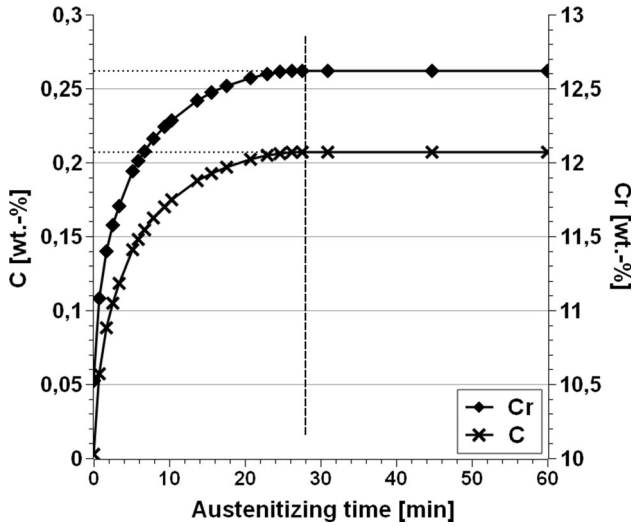

Fig. 12—Calculated concentrations of C and Cr in the austenite as a function of the austenitizing time. The dotted lines show the global composition.

proportions of the various alloying elements increase. Figures 12 and 13 show the chemical composition of austenite as a function of the austenitizing time. The solid lines show the calculated quantities of the alloying elements, the dotted lines show the respective global composition. It can be seen that the contents of the elements carbon and chromium increase continuously as $M_{23}C_6$ carbides are dissolved. The manganese content also increases slightly. The matrix concentrations of the elements silicon and nickel decreases slightly. In relation to the composition of the carbides previously present in the microstructure, this means that the carbides have contained significant amounts of carbon and chromium

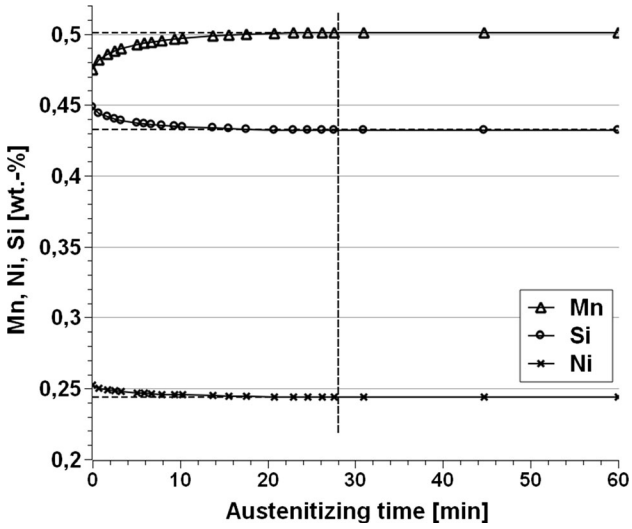

Fig. 13—Calculated concentrations of Mn, Si and Ni in the austenite as a function of the austenitizing time. The dotted lines show the global composition.

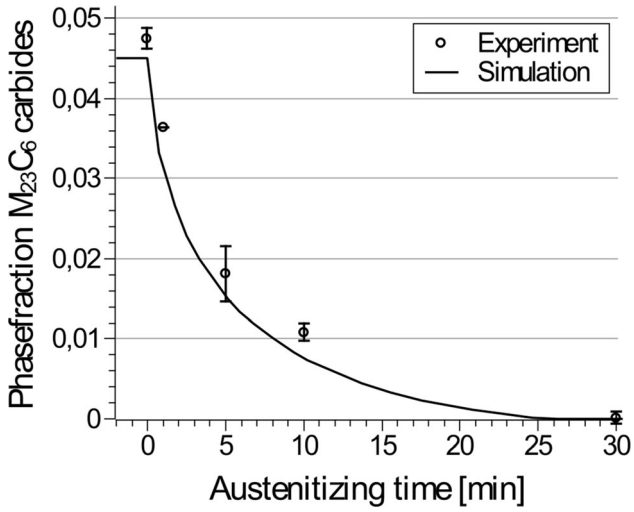

Fig. 14—Comparison of the calculated and measured phase quantities as a function of the austenitizing time for austenitizing at 1000 °C.

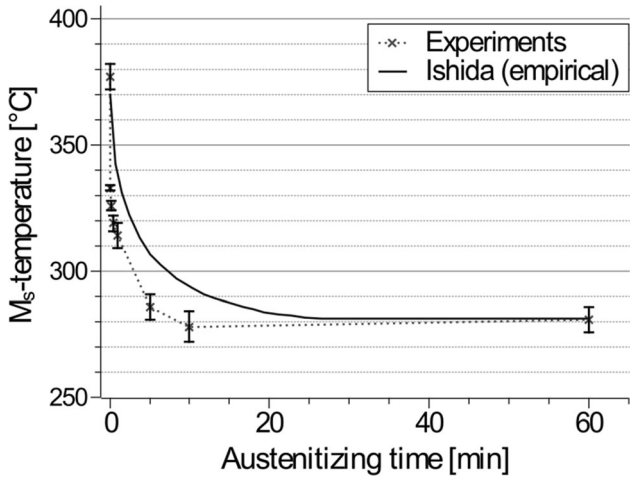

Fig. 15—Application of the empirically calculated M_s temperature according to Ishida[25] as a function of the austenitizing time. The measured M_s-temperatures are compared (2nd derivation). The dotted line does not correspond to the measured values between the points.

and small amounts of manganese. The elements nickel and silicon were not dissolved in the precipitates. With the help of the simulation model the chemical composition of the $M_{23}C_6$ carbides was also calculated. Because this carbide is considered as stoichiometric, the chemical composition does not change significantly depending on the austenitizing time.[23] The main components are 67.70 wt pct Cr, 25.52 wt pct Fe and 5.58 wt pct C. In addition, there are small amounts of manganese (1.17 wt pct). Compared to the chemical composition determined by XRD (see Results and discussion, first section), these simulation results are in good agreement. Again, like in the calculation of the phase fractions, an adjustment of the equilibrium is shown after 27 minutes. After this time at the temperature of 1000 °C all precipitates are dissolved, all alloying elements are dissolved in the austenite and thus the austenite is present in its equilibrium composition, neglecting local variation in fcc composition related to limited Cr diffusion and partitioning of C.

The results of the simulations are compared with the results of the experiments according to the chemical composition and the microstructure. The comparison of the calculated phase quantities as a function of the austenitizing time shows a good agreement with the measured phase contents (Figure 14. For an austenitizing time of 10 minutes, the largest deviation in the phase content was determined to be only 0.003. This difference can be explained by the preparation method. Etching the specimen exposes the carbides, resulting in two different height profiles while then the base plane is represented by the matrix. The carbides show a topographically elevated position, relative to the matrix. This offset cannot be accurately represented with an SEM due to the shallow depth of field.[24] If the matrix is in focus, carbides will inevitably appear larger because they are closer to the detector.

$$M_s(^\circ\mathrm{C}, \mathrm{wtpct}) = 545 - 330\,\mathrm{C} + 2\,\mathrm{Al} + 7\,\mathrm{Co} - 14\,\mathrm{Cr} - 13\,\mathrm{Cu} - 23\,\mathrm{Mn} - 5\,\mathrm{Mo} - 4\,\mathrm{Nb} - 13\,\mathrm{Ni} - 7\,\mathrm{Si} + 3\,\mathrm{Ti} + 4\,\mathrm{V} + 0\,\mathrm{W} \quad [1]$$

The chemical composition of austenite at austenitizing temperature could not be measured *in situ*. The martensite start temperature was determined instead as an indirect measure from the calculated composition using the empirical formula (Eq. [1]) according to Ishida.[25] The martensite start temperature is determined with the computed composition of the austenite (see Figures 12 and 13) and in this way the empirical temperatures can be compared with the measured temperatures. Figure 15

shows the curve of the calculated M_s-temperatures over the austenitizing time. The measured temperatures are plotted in the same Figure, which were determined with the aid of the second derivative. The individually measured values are interpolated by a dotted line. This does not show the real trend between the points, but only helps to compare the results. The M_s-temperatures for the equilibrium composition ($t_{aus} \geq 27$ minutes) are almost identical to the calculated ones and even with virtually no holding time at 1000 °C one can see a good agreement of the values. This shows that the selected empirical formula according to Ishida gives reliable results for the alloy investigated here. For austenitizing times between a few seconds and 10 to 15 minutes, however, the results show a deviation. The deviation is maximal at $t_{aus} = 5$ minutes. Here, the M_s temperature measured experimentally is up to 20 K below the empirically calculated one. With an associated standard deviation of 10 K at $t_{aus} = 5$ minutes, the difference considered is statistically significant, but nevertheless not very large. It is clear that the simulation model for calculating the chemical composition provides good but not yet exact results.

One reason for the deviation between the measured and the calculated martensite start temperatures is the chemical composition of the austenite. The simulation model considers the chemical composition globally. Locally, however, there are differences in the concentration of the different alloying elements, which is due to the dissolution of the carbides. If a carbide is dissolved, its radius is reduced and an enrichment of, *e.g.*, carbon and chromium is formed in the matrix in the immediate vicinity of the carbide.[26,27] Hosseini *et al.* showed in their work that the carbon gradient exhibits only small differences.[28] Already after a time of 100 μs carbon could be distributed further and lead to an almost homogeneous state. Chromium as a substitutionally dissolved element has a much lower diffusion coefficient than carbon and therefore needs much more time to redistribute homogeneously in the matrix. Moreover, as long as Cr is not homogeneously distributed within the austenitic matrix, carbon is expected to redistribute according to a paraequilibrium. Higher concentrations of carbon can be anticipated in Cr-enriched regions of the austenite. Schneider *et al.* also showed in their work by simulation that a gradient around the existing carbide can be detected up to a duration of over 150 hours.[7] The existence of this concentration difference inevitably leads to a different martensite start temperature, more precisely to locally different M_s values within the microstructure. A decreased martensite start temperature is to be expected at those positions where there is a local increase in alloying elements.[4,20,25] Since even small volumes that are converted to martensite mean an increase in volume relative to the entire sample,[1] these are detectable in the dilatometric tests. This effect is considered to explain the differences between the measured and calculated martensite start temperatures. The simulation model is able to determine the chemical composition of the austenite globally in a correct way. However, local changes resulting from the processes are not taken into account.

IV. CONCLUSIONS

The aim of this work was to investigate the microstructural processes during a short-term heat treatment process. For this purpose, experimental tests were carried out using a quenching dilatometer and the results were simulated with the commercial MatCalc Software. In summary, three core findings can be derived:

1. Phase quantities: With the help of the simulation model the occurring phase quantities of $M_{23}C_6$-carbides can be mapped well. Minor deviations result from the preparation methodology. Both the experiments and the simulation model show that after a holding time of about 30 minutes at 1000 °C all carbides are dissolved.
2. Chemical composition: For near-equilibrium conditions, the chemical composition of the austenite can be well represented. For metastable states, in which diffusion processes have a large local influence, the simulation model can only be used to a limited extent to reproduce the experiments. The model can only calculate global chemical compositions. The resulting local concentration differences of the alloying elements are not recorded and thus result in computational differences compared to the measurement in the experiment, which in this case are up to 20 K.
3. Martensite start: The experiments showed that the system under investigation shows a slow start phenomenon. This means that various methods, such as the tangent method or the offset method, are not suitable for determining M_s of the material which was considered in this study because they would show too large deviations. The newly developed method, in which the second derivative of the change in length as a function of temperature is investigated, achieves statistically significant measured values. The cause of the slow start phenomenon was not investigated further. Nevertheless, it is recommended to determine the M_s temperature in systems with such a phenomenon using the second derivative method.

With the investigations presented here it was shown that the microstructural processes during a short-term heat treatment of a martensitic stainless steel can be modeled in a simulation program with small uncertainties. Considering the limited local validity of the chemical composition, the simulation can be transferred to real experiments. Thus, a contribution can be made to reduce the experimental effort required to optimize a heat treatment even for very short periods of time.

FUNDING

Open Access funding enabled and organized by Projekt DEAL.

REFERENCES

1. H. Berns and W. Theisen: *Eisenwerkstoffe*, Stahl und Gusseisen, Springer Vieweg, 2008.
2. H.G. Bauer, W. Schadt, *Walzen von Flachprodukten* (Springer Verlag, 2017).
3. Z.-K. Liu, L. Hoglund, B. Jönsson, and J. Ågren: *Metall. Trans. A*, 1991, vol. 22A (8), pp. 1745–52.
4. U.R. Lenel and R.W.K. Honeycombe: *Metal Sci.*, 1984, vol. 18 (4), pp. 201–06.
5. C. Garcia, L. Alvarez, and M. Carsi: *Weld. Int.*, 1992, vol. 6 (8), pp. 612–21.
6. P. Rosemann, N. Kauss, C. Müller, T. Halle, Conference Paper: 16. Sommerkurs Werkstoffe und Fügen 71–78 (2017).
7. A. Schneider and G. Inden: *Acta Mater.*, 2015, vol. 53, pp. 519–31.
8. A. Kamyabi-Gol, D. Herath, and P.F. Mendez: *Can. Metal. Q.*, 2016, vol. 56 (1), pp. 85–93.
9. T. Sourmail and V. Smanio: *Mater. Sci. Technol.*, 2013, vol. 29 (7), pp. 883–88.
10. A. Kamyabi-Gol, S. Clark, J. Gibbs, S. Sridhar, and P. Mendez: *Acta Mater.*, 2015, vol. 102, pp. 231–40.
11. J. R. J. Marcuci, E. C. de Souza, C. C. Camilo, P. L. D. Lorenzo, J. ao Manuel Domingos de Almeida Rollo, Engenharia Biomédica 30 (3) (2014) 257–64.
12. T.A. Kop, J. Sietsma, and S. van der Zwaag: *J. Mater. Sci.*, 2001, vol. 36, pp. 519–26.
13. ASTM International, ASTM A1033-18 Standard Practice for Quantitative Measurement and Reporting of Hypoeutectoid Carbon and Low-Alloy Steel Phase Transformations 1 (2018).
14. H.S. Yang and H.K.D.H. Bhadeshia: *Mater. Sci. Technol.*, 2007, vol. 23 (5), pp. 556–60.
15. J. Orlich, H.-J. Pietrzeniuk, Atlas zur wärmebehandlung der stähle - band 4, 2. teil (1976).
16. L. Yuan, Nanoscale austenite reversion through partitioning, segregation and kinetic freezing in martensitic stainless steels, Dissertation, RWTH Aachen, (2012).
17. C.G. de Andrés, F. Caballero, C. Capdevila, and L. Álvarez: *Mater. Charact.*, 2002, vol. 48, pp. 101–11.
18. C.G. de Andrés, J. Jiménez, and L. Álvarez: *Metall. Mater. Trans. A*, 1996, vol. 31 (1), pp. 53–74.
19. G. Gottstein, Materialwissenschaften und Werkstofftechnik - Physikalische Grundlagen, Springer Vieweg, (2014).
20. G. B. Olson, W. S. Owen (Eds.), Martensitic Nucleation, ASM International, 1992, Ch. 9, pp. 149–74.
21. O.D. Sherby, J. Wadsworth, D.R. Lesuer, and C.K. Syn: *Mater. Trans.*, 2008, vol. 49 (9), pp. 2016–27.
22. M. Belde, H. Springer, G. Inden, and D. Raabe: *Acta Mater.*, 2015, vol. 86, pp. 1–14.
23. A.M. Bettanini, L. Ding, J.-D. Mithieux, C. Parrens, H. Idrissi, D. Schryvers, L. Delannay, T. Pardoen, and P.J. Jacques: *Mater. Des.*, 2019, vol. 162, pp. 362–74.
24. M. Hemmleb, Photogrammetrische auswertung elektronenmikroskopischer bilddaten, Dissertation, TU Berlin, (2001).
25. K. Ishida: *J. Alloys Compd.*, 1995, vol. 220, pp. 126–34.
26. A. Bjärbo and M. Hättestrand: *Metall. Mater. Trans. A*, 1999, vol. 32, pp. 19–27.
27. S. Papaefthymiou, M. Bouzouni, and R.H. Petrov: *Metals*, 2018, vol. 8 (8), p. 646.
28. S.B. Hosseinia, R. Dahlgrena, K. Ryttbergb, and U. Klemen: *Proc. CIRP*, 2014, vol. 14, pp. 107–12.